A discrete numerical model for granular assemblies

P. A. CUNDALL* and O. D. L. STRACK†

The distinct element method is a numerical model capable of describing the mechanical behaviour of assemblies of discs and spheres. The method is based on the use of an explicit numerical scheme in which the interaction of the particles is monitored contact by contact and the motion of the particles modelled particle by particle. The main features of the distinct element method are described. The method is validated by comparing force vector plots obtained from the computer program BALL with the corresponding plots obtained from a photoelastic analysis. The photoelastic analysis used for the comparison is the one applied to an assembly of discs by De Josselin de Jong and Verruijt (1969). The force vector diagrams obtained numerically closely resemble those obtained photoelastically. It is concluded from this comparison that the distinct element method and the program BALL are valid tools for research into the behaviour of granular assemblies.

La méthode des éléments distincts est un modèle numérique capable de décrire le comportement mécanique de l'assemblage de disques et de sphères. La méthode est basée sur l'utilisation d'un système numérique explicite dans lequel l'interaction des particules est contrôlée contact par contact et le mouvement des particules simulé particule par particule. Les caracteristiques principales de la méthode des éléments distints sont décrites. La méthode est validée en comparant les tracés de vecteur de force obtenus par le programme sur ordicateur BALL avec les tracés correspondants obtenus à l'aide d'une analyse photo-élastique. L'analyse photo-élastique utilisée pour la comparaison est celle appliquée sur un assemblage de disques par De Josselin de Jong et Verruijt (1969). Les diagrammes de vecteur de force obtenus numériquement sont très voisins de ceux obtenus photo-élastiquement. Cette comparaison permet de conclure que la methode des éléments distincts et le programme BALL sont des instruments valables pour la recherche du comportement des assemblages granulaires.

INTRODUCTION

A granular medium is composed of distinct particles which displace independently from one another and interact only at contact points. The discrete character of the medium results in a complex behaviour under conditions of loading and unloading and to date no satisfactory constitutive relationships have been established. Extensive programmes of laboratory tests are necessary to generate new constitutive relations or to validate existing ones.

Interpretation of tests on real granular media, such as sand, is difficult because the stresses inside the sample cannot be measured and must be estimated from the boundary conditions. New experimental techniques using x-ray photography make measurements of strains possible but no such techniques exist for the determination of stresses within a sand sample.

The uncertainties regarding interior stresses in samples of sand have led to the development of models of granular media that are geometrically simpler than sand and for which the stresses and displacements can either be calculated or measured. These models consist of assemblies of discs or spheres and may be analytical, physical or numerical.

An analytical model for cubic arrays of spheres of uniform size was proposed by Deresiewicz (1958). The resulting expressions predict a non-linear and hysteretic stress–strain behaviour. Ultimate failure is also accommodated in the formulation. The analytic approach, however, is restricted in that the array is cubic, the spheres are uniform in size and the loading sequence is limited.

A testing technique for assemblies of discs that makes possible the direct determination of contact forces between the particles was proposed by Dantu (1957) and Wakabayashi (1957). These investigators suggested the use of optically sensitive material for the discs. Analysis of the force distribution in such a test was described by De Josselin de Jong and Verruijt (1969). Although testing of assemblies of photoelastic discs is quite general and allows for an accurate determination of contact forces and of displacements and rotations of the individual discs, the analysis is time-consuming. Drescher and De Josselin de Jong (1971) performed a series of such tests in order to verify De Josselin de Jong's double-sliding free-rotating model. The information extracted from these tests was sufficient to confirm the main features of the continuum model.

Possibly the most powerful way of modelling assemblies of discs and spheres is by numerical techniques. Numerical modelling is more flexible in application than analytical modelling and has the advantage over physical modelling that any data are accessible at any stage of the test. The flexibility of numerical modelling extends to loading configurations, particle sizes, size distributions and physical properties of the particles.

Serrano and Rodriguez-Ortiz (1973) and Rodriguez-Ortiz (1974) developed a numerical model for assemblies of discs and spheres. Contact forces and displacements are calculated for equilibrium conditions assuming that increments of contact forces are determined by incremental displacements of the particle centres. Herzian-type contact compliances are used for normal forces, the effects of tangential forces are considered according to the theories of Mindlin and Deresiewicz (1953) and Nayak (1972), and shape changes are negligible. A major drawback of the method used to solve the equations is that only a relatively small number of particles can be processed by the present computers. In addition, the calculation is time-consuming because the matrix representing the contact stiffnesses must be reformulated whenever a contact is made or broken.

The distinct element method is a numerical model that is capable of handling particles of any shape and was developed by Cundall (1971 and 1974) for the analysis of rock mechanics problems. In the distinct element method, the interaction of the particles is viewed as a transient problem with states of equilibrium developing whenever the internal forces balance. The numerical scheme is explicit and the consequent efficiency in the use of memory space is such that problems involving about 1500 particles can be accommodated in the core memory of a mini computer with a memory of 64 K of 32-bit words.

It is the main objective of the Paper to show that the distinct element method models the behaviour of assemblies of discs realistically. This is done by the independent numerical reproduction of a test on an assembly of discs reported by De Josselin de Jong and Verruijt (1969). A comparison between the numerical results and the results of the photoelastic disc tests indicates that the numerical model may be used to replace tests on photoelastic discs. The numerical model is proposed as a new tool for fundamental research into the behaviour of two-dimensional assemblies of discs.

THE DISTINCT ELEMENT METHOD

The principles on which the distinct element method is based and the nature of the fictitious material which may be modelled by this method are discussed below. The reader is referred to Cundall (1978) for a more detailed description of the method and of the computer program BALL developed for modelling two-dimensional assemblies of discs.

In the distinct element method, the equilibrium contact forces and displacements of a stressed assembly of discs are found through a series of calculations tracing the movements of the individual particles. These movements are the result of the propagation through the medium of

disturbances originating at the boundaries: a dynamic process. The speed of propagation is a function of the physical properties of the discrete medium.

In describing the above dynamic behaviour numerically, time steps are taken over which velocities and accelerations are assumed to be constant. The distinct element method is based upon the idea that the time step chosen may be so small that during a single time step disturbances cannot propagate from any disc further than its immediate neighbours. Then, at all times the resultant forces on any disc are determined exclusively by its interaction with the discs with which it is in contact. It is this key feature of the distinct element method which makes it possible to follow the non-linear interaction of a large number of discs without excessive memory requirements or the need for an iterative procedure. It should be noted that all analyses presented in this Paper are for dry assemblies, and deal with total contact forces. A technique that has been devised for accommodating pore pressures will be described in a later publication.

The calculation cycle

The calculations performed in the distinct element method alternate between the application of Newton's second law to the discs and a force–displacement law at the contacts. Newton's second law gives the motion of a particle resulting from the forces acting on it. The force–displacement law is used to find contact forces from displacements.

The deformations of the individual particles are small in comparison with the deformation of a granular assembly as a whole. The latter deformation is due primarily to the movements of the particles as rigid bodies. Therefore, precise modelling of particle deformation is not necessary to obtain a good approximation of the mechanical behaviour. In the current version of BALL, the particles are allowed to overlap one another at contact points. This overlapping behaviour takes the place of the deformation of the individual particles. The magnitude of the overlap is related directly to the contact force in the way explained below. It should be noted, however, that these overlaps are small in relation to the particle sizes.

To illustrate how forces and displacements are determined during a calculation cycle, the case represented in Fig. 1(a) will be considered. Two weightless discs, labelled as disc x and disc y, are squashed between a pair of rigid walls. The walls move toward each other at a constant velocity v. Initially, at time $t = t_0$, the walls and discs are touching and no contact forces exist. A time Δt later, the walls have moved inward over distances $v\Delta t$. In accordance with the assumption that the disturbances cannot travel beyond a single disc during one time step, both discs are assumed to maintain their initial positions during the time interval from $t = t_0$ to $t = t_0 + \Delta t$. Overlaps therefore exist at time $t_1 = t_0 + \Delta t$ at contacts A and C (see Fig. 1(b)) and are of magnitude $\Delta n = v\,\Delta t$.

Points $A_{(D)}$ and $A_{(w)}$ (see Fig. 1(b)) are points of the disc and the wall, respectively, lying on the line drawn perpendicular to the wall and through the centre of the disc. The contact A is defined as the point halfway between $A_{(D)}$ and $A_{(w)}$. The relative displacement $(\Delta n_{(A)})_{t1}$ at the contact (the overlap) is defined as the displacement of point $A_{(w)}$ relative to that of point $A_{(D)}$ occurring over one time increment. The subscript $t1$ in $(\Delta n_{(A)})_{t1}$ refers to time.

The relative displacements occurring at contacts A and C at time $t_1 = t_0 + \Delta t$ (see Fig. 1(b)) are used in a force–displacement law for the calculation of contact forces. In the present version of the computer program BALL, an incremental force–displacement law of the following form is used

$$\Delta F_n = k_n(\Delta n)_{t1} = k_n v\,\Delta t \quad\quad\quad\quad (1)$$

where k_n is the normal stiffness and ΔF_n represents the increment in normal force.

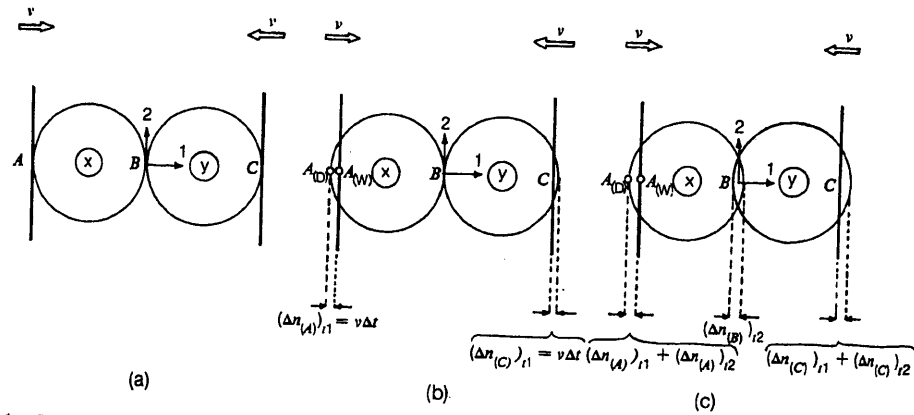Defining the positive 1 direction as pointing from disc x to disc y (see Fig. 1(b)) the sums of

Fig. 1. Two discs compressed between rigid walls (the overlaps are exaggerated); (a) $t = t_0$: (b) $t = t_1 = t_0 + \Delta t$: (c) $t = t_2 = t_0 + 2\Delta t$

force $F_{(x)1}$ and $F_{(y)1}$ for discs x and y at time $t_1 = t_0 + \Delta t$ become, taking $F_{(x)1}$ and $F_{(y)1}$ to be positive in the positive 1 direction,

$$F_{(x)1} = k_n (\Delta n)_{t1}, \quad F_{(y)1} = -k_n (\Delta n)_{t1} \quad \ldots \ldots \quad (2)$$

These forces are used to find new accelerations using Newton's second law

$$\ddot{x}_1 = F_{(x)1}/m_{(x)}, \quad \ddot{y}_1 = F_{(y)1}/m_{(y)} \quad \ldots \ldots \ldots \quad (3)$$

where $\ddot{x}_1$ and $\ddot{y}_1$ stand for the respective accelerations of discs x and y in the 1 direction and where the subscripts (x) and (y) in the masses $m_{(x)}$ and $m_{(y)}$ refer to discs x and y. The accelerations found from equation (3) are assumed to be constant over the time interval from $t_1 = t_0 + \Delta t$ to $t_2 = t_0 + 2\Delta t$ and may be integrated to yield velocities

$$[\dot{x}_1]_{t2} = [F_{(x)1}/m_{(x)}]\Delta t, \quad [\dot{y}_1]_{t2} = [F_{(y)1}/m_{(y)}]\Delta t \quad \ldots \ldots \quad (4)$$

The relative displacement increments at contacts A, B and C at time $t_2 = t_0 + 2\Delta t$ are found from

$$(\Delta n_{(A)})_{t2} = (v - [F_{(x)1}/m_{(x)}]\Delta t)\Delta t \quad \ldots \ldots \ldots \ldots \quad (5)$$

$$(\Delta n_{(B)})_{t2} = ([F_{(x)1}/m_{(x)}]\Delta t - [F_{(y)1}/m_{(y)}]\Delta t)\Delta t \quad \ldots \ldots \quad (6)$$

$$(\Delta n_{(C)})_{t2} = ([F_{(y)1}/m_{(y)}]\Delta t - [-v])\Delta t \quad \ldots \ldots \ldots \ldots \quad (7)$$

where $\Delta n_{(A)}$, $\Delta n_{(B)}$ and $\Delta n_{(C)}$ are taken as positive for compression.

This cycle may be repeated again and again: forces corresponding to the displacements are found using the force displacement law, equation (2), and the force sums for the two discs are substituted in Newton's second law, equation (3), to obtain displacements.

The above example is an illustration of the cycling through a force–displacement law and the law of motion. In the general case of an assembly of many discs, the force–displacement law is applied at each contact of any disc and the vectorial sum of these contact forces is determined to yield the resultant force acting on that disc. When this has been accomplished for every disc, new accelerations are calculated from Newton's second law. The equations used in a calculation cycle for a general assembly are presented in the following section.

The force–displacement law

The force–displacement law will be presented for the case of two discs in contact, discs x and

---

Fig. 2. The for

y in Fig. 2. T
y_2) where the
indicated in I
$\dot{y}_i = (\dot{y}_1, \dot{y}_2)$
direction, wh
$R_{(x)}$ and $R_{(y)}$
section of the

Two discs
the sum of th

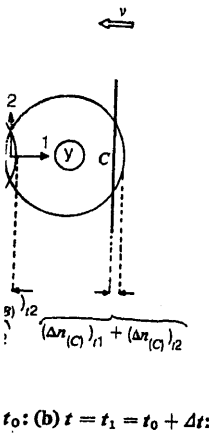If this conditi
integration o
of point $P_{(x)}$
as pointing fr

and the unit

The relativ

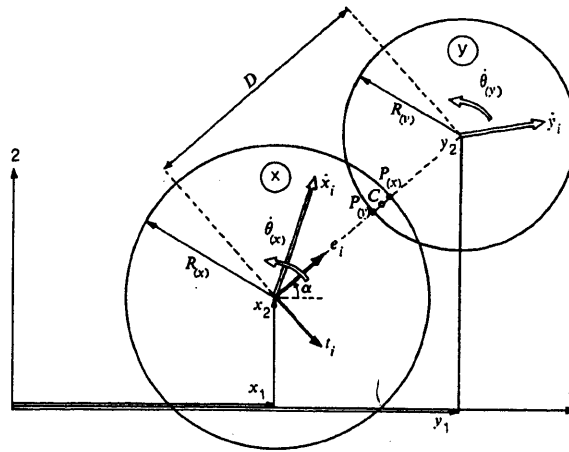The norma
$\dot{X}_i$ onto e_i an

and

$\dot{s} =$

Fig. 2.   The force–displacement law

y in Fig. 2. The co-ordinates of the disc centres are represented as $x_i = (x_1, x_2)$ and $y_i = (y_1, y_2)$ where the indices 1 and 2 refer to the co-ordinates of a Cartesian co-ordinate system as indicated in Fig. 2. The components of the velocity vectors of discs x and y are $\dot{x}_i = (\dot{x}_1, \dot{x}_2)$, $\dot{y}_i = (\dot{y}_1, \dot{y}_2)$ and the angular velocities are $\dot{\theta}_{(x)}$ and $\dot{\theta}_{(y)}$, taken positive in counterclockwise direction, where the dots stand for differentiation with respect to time. Discs x and y have radii $R_{(x)}$ and $R_{(y)}$ and masses $m_{(x)}$ and $m_{(y)}$. Points $P_{(x)}$ and $P_{(y)}$ are defined as the points of intersection of the line connecting the disc centres with the boundaries of discs x and y, respectively.

Two discs are taken to be in contact only if the distance D between their centres is less than the sum of their radii, i.e. if

$$D < R_{(x)} + R_{(y)} \quad . \qquad . \qquad . \qquad . \qquad . \qquad . \qquad . \qquad (8)$$

If this condition is met, the relative displacement at the contact C (see Fig. 2) is determined by integration of the relative velocity. The relative velocity at the contact is defined as the velocity of point $P_{(x)}$ with respect to $P_{(y)}$. The unit vector $e_i = (\cos \alpha, \sin \alpha)$ (see Fig. 2) is introduced as pointing from the centre of disc x to the centre of disc y, i.e.

$$e_i = \frac{y_i - x_i}{D} = (\cos \alpha, \sin \alpha) \quad . \qquad . \qquad . \qquad . \qquad . \qquad . \qquad (9)$$

and the unit vector t_i is obtained by a clockwise rotation of e_i through 90°, i.e.

$$t_i = (e_2, -e_1) \quad . \qquad . \qquad . \qquad . \qquad . \qquad . \qquad . \qquad (10)$$

The relative velocity of point $P_{(x)}$ with recpect to $P_{(y)}$ now may be expressed as $\dot{X}_i$ with

$$\dot{X}_i = (\dot{x}_i - \dot{y}_i) - (\dot{\theta}_{(x)} R_{(x)} + \dot{\theta}_{(y)} R_{(y)}) t_i \quad . \qquad . \qquad . \qquad . \qquad (11)$$

The normal ($\dot{n}$) and tangential ($\dot{s}$) components of the relative velocities are the projections of $\dot{X}_i$ onto e_i and t_i, respectively,

$$\dot{n} = \dot{X}_i\, e_i = (\dot{x}_i - \dot{y}_i) e_i - (\dot{\theta}_{(x)} R_{(x)} + \dot{\theta}_{(y)} R_{(y)}) t_i\, e_i = (\dot{x}_i - \dot{y}_i) e_i \quad . \qquad . \qquad (12)$$

and

$$\dot{s} = \dot{X}_i t_i = (\dot{x}_i - \dot{y}_i) t_i - (\dot{\theta}_{(x)} R_{(x)} + \dot{\theta}_{(y)} R_{(y)}) t_i t_i = (\dot{x}_i - \dot{y}_i) t_i - (\dot{\theta}_{(x)} R_{(x)} + \dot{\theta}_{(y)} R_{(y)}) \quad . \qquad (13)$$
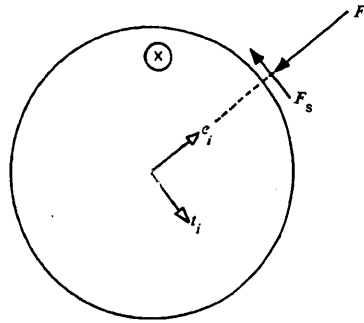
Fig. 3. Sign convention for F_n and F_s.

where the Einstein summation convention is adopted for the index i; i.e. the summation is performed over the index that occurs twice in each expression (indices in parentheses are not summed). Integration of the relative velocity component with respect to time gives the components Δn and Δs of the relative displacement increment

and

$$\Delta n = (\dot{n})\Delta t = \{(\dot{x}_i - \dot{y}_i)e_i\}\Delta t \quad . \quad . \quad . \quad . \quad . \quad . \quad (14)$$

$$\Delta s = (\dot{s})\Delta t = \{(\dot{x}_i - \dot{y}_i)t_i - (\dot{\theta}_{(x)}R_{(x)} + \dot{\theta}_{(y)}R_{(y)})\}\Delta t \quad . \quad . \quad . \quad (15)$$

These relative displacement increments are used, with the force–displacement law to calculate increments of the normal and shear forces, ΔF_n and ΔF_s

and

$$\Delta F_n = k_n \Delta n = k_n\{(\dot{x}_i - \dot{y}_i)e_i\}\Delta t \quad . \quad . \quad . \quad . \quad . \quad (16)$$

$$\Delta F_s = k_s \Delta s = k_s\{(\dot{x}_i - \dot{y}_i)t_i - (\dot{\theta}_{(x)}R_{(x)} + \dot{\theta}_{(y)}R_{(y)})\}\Delta t \quad . \quad . \quad . \quad (17)$$

where k_n and k_s represent the normal and shear stiffnesses, respectively.

Finally, at each time step the force increments ΔF_n and ΔF_s are added into the sum of all force increments, F_n and F_s, determined for previous time steps:

$$(F_n)_N = (F_n)_{N-1} + \Delta F_n; \quad (F_s)_N = (F_s)_{N-1} + \Delta F_s \quad . \quad . \quad . \quad . \quad (18)$$

where the indices N and $N-1$ refer to times t_N and t_{N-1} such that $t_N - t_{N-1} = \Delta t$. The sign convention for the normal and shear forces acting on disc x is as indicated in Fig. 3: F_n and F_s are taken as positive in the directions opposite to e_i and t_i.

A Coulomb-type friction law is incorporated as follows. The magnitude of the shear force F_s found from equation (18) is checked against the maximum possible value $(F_s)_{max}$ defined as

$$(F_s)_{max} = F_n \tan \phi_\mu + c \quad . \quad . \quad . \quad . \quad . \quad . \quad (19)$$

where ϕ_μ is the smaller of the interparticle friction angles of the two discs in contact and c the smaller of their cohesions.[1] If the absolute value of $(F_s)_N$ as found from equation (18) is larger than $(F_s)_{max}$, $(F_s)_N$ is set equal to $(F_s)_{max}$, preserving the sign obtained from equation (18).

---

[1] This scheme was used for programming convenience when running problems with only two different friction angles: one for particle-to-particle contact, the other for particle-to-wall contact. For problems involving many dissimilar particles the program could be modified quite easily to associate each value of ϕ_μ and c with a particular type of contact rather than with a particular type of particle.

Once the no
disc x, they ar
force compon
on disc x, Σ
from $\Sigma M_{(x)} =$

The resulta
determine the

Motion

The velocit
obtained as f
act on disc x

where $I_{(x)}$ rep
step Δt, equa

These equa
may be used

The new v
by a further

The finite di

Body forc
term $m_{(x)}g_i$
the two com

Damping

Friction d
contact is (F

The prog
to be referre
relative velo
the normal
not applied

The coeffi
by c_n and c
in the force

and

Once the normal and shear forces have been determined for each contact of a disc, for example disc x, they are resolved into components in the 1 and 2 directions. The sum of these contact force components gives the resultant forces $\Sigma F_{(x)1}$ and $\Sigma F_{(x)2}$. The resultant moment acting on disc x, $\Sigma M_{(x)}$ is taken positive if acting in the counterclockwise direction and is found from $\Sigma M_{(x)} = \Sigma F_s R_{(x)}$ where summation is taken over all contacts of disc x.

The resultant moments and forces acting on disc x are used with Newton's second law to determine the new accelerations $\ddot{x}_i$ and $\ddot{\theta}_{(x)}$.

Motion

The velocities $\dot{x}_i$ and $\dot{\theta}_{(x)}$ used in the force–displacement law in equations (16) and (17) are obtained as follows. The current resultant force and the moment at time t_N are assumed to act on disc x during the interval Δt from $t_{N-\frac{1}{2}}$ to $t_{N+\frac{1}{2}}$. Newton's second law applied to disc x is

$$m_{(x)}\ddot{x}_i = \Sigma F_{(x)i} \qquad \ldots \ldots \ldots \quad (20)$$

$$I_{(x)}\ddot{\theta}_{(x)} = \Sigma M_{(x)} \qquad \ldots \ldots \ldots \quad (21)$$

where $I_{(x)}$ represents the moment of inertia of disc x. Taking $\ddot{x}_i$ and $\ddot{\theta}_{(x)}$ constant over the time step Δt, equations (20) and (21) lead to the following expressions for the velocities

$$(\dot{x}_i)_{N+\frac{1}{2}} = (\dot{x}_i)_{N-\frac{1}{2}} + [\Sigma F_{(x)i}/m_{(x)}]_N \Delta t \quad \ldots \ldots \quad (22)$$

$$(\dot{\theta}_{(x)})_{N+\frac{1}{2}} = (\dot{\theta}_{(x)})_{N-\frac{1}{2}} + [\Sigma M_{(x)}/I_{(x)}]_N \Delta t \quad \ldots \ldots \quad (23)$$

These equations are applied to each disc in turn. These new values for the velocities now may be used in the force–displacement law and the cycle repeated for a new time increment.

The new values for velocities are used also to update the positions and rotations of the discs by a further numerical integration

$$(x_i)_{N+1} = (x_i)_N + (\dot{x}_i)_{N+\frac{1}{2}} \Delta t \qquad \ldots \ldots \ldots \quad (22a)$$

$$(\theta_{(x)})_{N+1} = (\theta_{(x)})_N + (\dot{\theta}_{(x)})_{N+\frac{1}{2}} \Delta t \qquad \ldots \ldots \ldots \quad (23a)$$

The finite difference equations (22), (22a), (23), (23a) represent a time–centred system.

Body forces, such as gravitational forces, may be incorporated, if so desired. In that case a term $m_{(x)}g_i$ is added to the force sum $\Sigma F_{(x)i}$ in equation (22), where $g_i = (g_1, g_2)$ represents the two components of the acceleration vector due to the body force.

Damping

Friction damping occurs during sliding when the absolute value of the shear force at any contact is $(F_s)_{max}$.

The program BALL further contains the option to include two forms of viscous damping to be referred to as contact damping and global damping. Contact damping operates on the relative velocities at the contacts and may be envisioned as resulting from dashpots acting in the normal and shear directions at the contacts. The viscous damping in the shear direction is not applied when sliding occurs. In this case friction damping alone operates.

The coefficients of viscous contact damping in the normal and shear directions are represented by c_n and c_s. If contact damping is taken into account, the damping forces must be included in the force-sums in equations (22) and (23), which become

$$(\dot{x}_i)_{N+\frac{1}{2}} = (\dot{x}_i)_{N-\frac{1}{2}} + \{\Sigma [F_{(x)i} + D_{(x)i}]/m_{(x)}\}_N \Delta t \quad \ldots \ldots \quad (24)$$

and

$$(\dot{\theta}_{(x)})_{N+\frac{1}{2}} = (\dot{\theta}_{(x)})_{N-\frac{1}{2}} + \{\Sigma M_{(x)}/I_{(x)}\}_N \Delta t \quad \ldots \ldots \quad (25)$$

where $\Sigma D_{(x)i}$ represents the sum of the components of the contact damping forces and where $\Sigma M_{(x)}$ now includes the contribution of the contact damping forces to the moment sum. The global components $D_{(x)i}$ are found from the normal (D_n) and shear (D_s) components of the damping force at the contacts, which are obtained from the following equations (see equations (12) and (13))

$$(D_n)_N = c_n \dot{n} = c_n[\dot{x}_i - \dot{y}_i]_{N-\frac{1}{2}} e_i \quad . \quad . \quad . \quad . \quad . \quad . \quad (26)$$

and

$$(D_s)_N = c_s \dot{s} = c_s[(\dot{x}_i - \dot{y}_i)_{N-\frac{1}{2}} t_i - (\theta_{(x)}R_{(x)} + \theta_{(y)}R_{(y)})_{N-\frac{1}{2}}] \quad . \quad . \quad . \quad (27)$$

There is an error of half a time-step in the calculation of D_n and D_s, but its effects have been found to be negligible.

In the current version of BALL, the contact damping coefficients c_n and c_s are taken to be proportional to the stiffnesses k_n and k_s with proportionality constant β,

$$c_n = \beta k_n, \quad c_s = \beta k_s \quad . \quad . \quad . \quad . \quad . \quad . \quad . \quad (28)$$

Global damping operates on the absolute velocities of the discs and is introduced in the calculations of motion. Global damping as incorporated in BALL may be envisioned as the effect of dashpots connecting each particle to ground. These dashpots operate both on the velocity vector components and on the rotational velocity.

If global damping is included in addition to contact damping, the equations of motion, (20) and (21), become (cf. equations (24) and (25)),

$$m_{(x)}\ddot{x}_i = \Sigma [F_{(x)i} + D_{(x)i}] - C\dot{x}_i \quad . \quad . \quad . \quad . \quad . \quad . \quad (29)$$

$$I_{(x)}\ddot{\theta}_{(x)} = \Sigma M_{(x)} - C^*\dot{\theta}_{(x)} \quad . \quad . \quad . \quad . \quad . \quad . \quad (30)$$

where C and C^* are the coefficients of global damping operating, respectively, on $\dot{x}_i$ and $\dot{\theta}_{(x)}$. A central difference scheme is used to integrate equations (29) and (30), whereby velocities are evaluated halfway through the time step, i.e.

$$(\dot{x}_i)_N = \tfrac{1}{2}[(\dot{x}_i)_{N-\frac{1}{2}} + (\dot{x}_i)_{N+\frac{1}{2}}], \quad (\dot{\theta}_{(x)})_N = \tfrac{1}{2}[(\dot{\theta}_{(x)})_{N-\frac{1}{2}} + (\dot{\theta}_{(x)})_{N+\frac{1}{2}}] \quad . \quad . \quad (31)$$

Writing $\ddot{x}_i$ as $[(\dot{x}_i)_{N+\frac{1}{2}} - (\dot{x}_i)_{N-\frac{1}{2}}]/\Delta t$ and $\ddot{\theta}_{(x)}$ as $[(\dot{\theta}_{(x)})_{N+\frac{1}{2}} - (\dot{\theta}_{(x)})_{N-\frac{1}{2}}]/\Delta t$ and using equation (31), equations (29) and (30) may be solved for $(\dot{x}_i)_{N+\frac{1}{2}}$ and $(\dot{\theta}_{(x)})_{N+\frac{1}{2}}$.

$$(\dot{x}_i)_{N+\frac{1}{2}} = \left\{(\dot{x}_i)_{N-\frac{1}{2}}\left[1 - \frac{C}{m_{(x)}}\frac{\Delta t}{2}\right] + \Sigma (F_{(x)i} + D_{(x)i})_N \frac{\Delta t}{m_{(x)}}\right\} \bigg/ \left\{1 + \frac{C}{m_{(x)}}\frac{\Delta t}{2}\right\} \quad . \quad (32)$$

and

$$(\dot{\theta}_x)_{N+\frac{1}{2}} = \left\{(\dot{\theta}_{(x)})_{N-\frac{1}{2}}\left[1 - \frac{C^*}{I_{(x)}}\frac{\Delta t}{2}\right] + (\Sigma M_{(x)})_N \frac{\Delta t}{I_{(x)}}\right\} \bigg/ \left\{1 + \frac{C^*}{I_{(x)}}\frac{\Delta t}{2}\right\} \quad . \quad (33)$$

In BALL, the coefficients C and C^* of global damping are taken to be proportional to mass and moment of inertia, respectively

$$C = \alpha m_{(x)}, \quad C^* = \alpha I_{(x)} \quad . \quad . \quad . \quad . \quad . \quad . \quad (34)$$

Using equation (34), equations (32) and (33) may be simplified to

$$(\dot{x}_i)_{N+\frac{1}{2}} = \left\{(\dot{x}_i)_{N-\frac{1}{2}}\left[1 - \alpha\frac{\Delta t}{2}\right] + \Sigma (F_{(x)i} + D_{(x)i})_N \frac{\Delta t}{m_{(x)}}\right\} \bigg/ \left\{1 + \alpha\frac{\Delta t}{2}\right\} \quad . \quad . \quad (35)$$
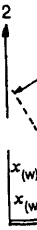
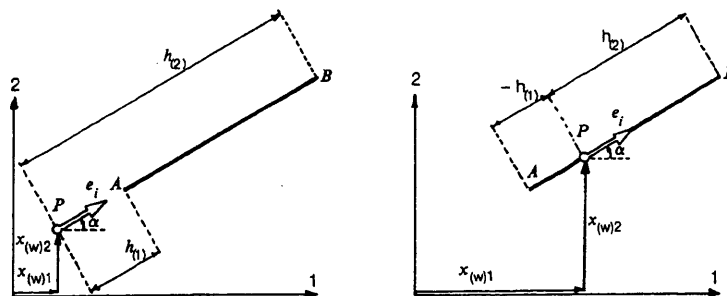**Fig. 4. Possible wall definitions**

and

$$(\theta_{(x)})_{N+\frac{1}{2}} = \left\{(\theta_{(x)})_{N-\frac{1}{2}}\left[1-\alpha\frac{\Delta t}{2}\right]+(\Sigma M_{(x)})_N\frac{\Delta t}{I_{(x)}}\right\}\Big/\left\{1+\alpha\frac{\Delta t}{2}\right\} \quad \cdot \quad \cdot \quad (36)$$

These equations for force–displacement and motion fully describe the BALL model of a granular material. Energy is dissipated in the model only through friction, contact and global damping. The use of damping other than by friction is necessary in order that the assemblies reach a state of equilibrium for all conditions. If neither contact nor global damping were included, the assemblies would not be able to reach exact equilibrium, but in practice the departure from equilibrium may be made as small as desired by reducing the applied loading rate. It may be noted that the linear force–displacement law discussed above is not inherent in the method. A non-linear law, such as that of Herzian contact, could equally well be employed.

The numerical scheme will be stable only if the time step Δt is taken as a fraction less than one of the critical time step, a result of the explicit nature of the model. An estimated value for the critical time step is determined in the program (see Cundall, 1978) and the user specifies the fraction of this time step that is to be used for the calculations. The critical time step is estimated on the basis of the single degree-of-freedom system of a mass m connected to ground by a spring of stiffness k, for which the critical time step equals $2\sqrt{(m/k)}$.

To illustrate how the program calculates and what effect variations in the physical properties specified by the user have on the output of the program, the results of some simple tests on nine discs are presented after a brief discussion of the input parameters.

Input parameters

The input parameters that must be specified to run numerical tests with BALL may be divided into two groups. One group consists of geometrical data and the other of physical properties data.

The geometrical data describe the positions and orientations of the straight rigid boundaries (the walls) and the positions and radii of the discs, with respect to a global co-ordinate system $(1, 2)$. A typical wall is defined in terms of a fixed point P with co-ordinates $x_{(w)i} = (x_{(w)1}, x_{(w)2})$ (see Fig. 4) and a unit vector $e_i = (\cos \alpha, \sin \alpha)$ such that the wall is a portion of the line passing through P and of the direction of e_i. Scalar multipliers of e_i, $h_{(1)}$ and $h_{(2)}$ define the wall endpoints A and B with co-ordinates $x_{(A)i} = x_{(w)i}+h_{(1)} e_i$ and $x_{(B)i} = x_{(w)i}+h_{(2)} e_i$, respectively.

The boundary conditions are of the strain-controlled type. The motion of the wall is specified rather than the forces applied to it. Movement of the wall is defined in terms of the velocity of
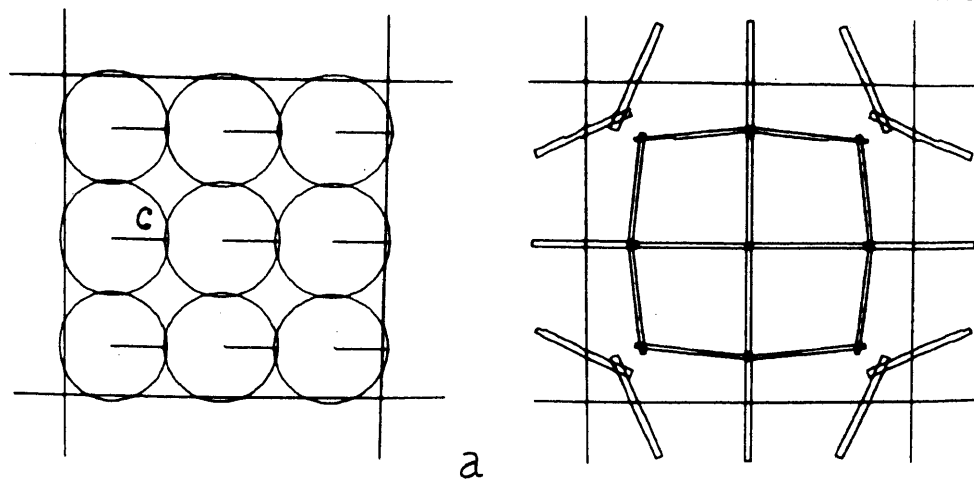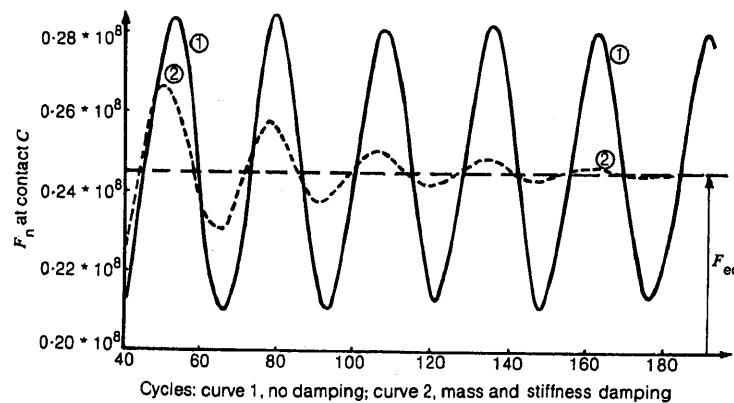
Fig. 5. Nine disc test

Cycles: curve 1, no damping; curve 2, mass and stiffness damping

Fig. 6. Damping effects

point P, $\dot{x}_{(w)i} = (\dot{x}_{(w)1}, \dot{x}_{(w)2})$ and the angular velocity of the wall about P, $\dot{\alpha}$. Defining a disc requires only that the disc centre and radius be specified.

For the purpose of assigning physical properties to the discs and walls, they are divided into groups such that all entries of a group have the same properties. Assigning a single type number to each disc or wall is then sufficient to associate with it the appropriate set of properties. The physical properties treated in this way include disc radius, density, cohesion, interparticle friction coefficient tan ϕ_μ, shear stiffness and normal stiffness (see footnote 1). There are other parameters that apply to the field as a whole, defining the contact damping, global damping and the fraction of the critical time step.

Units

The numerical values for density, stiffness and damping coefficients have been selected such that the overlaps are small in relation to the particle sizes, that the numerical process is stable and that the numerical values calculated in the program are in a range that can be handled with accuracy. No attempts have been made to relate the units used in BALL to physical units

---

in the examp
used in BAL
This is done
forces (see Fi
in contact ar
produced in
(see De Joss

The value:
the interpart
ing to analyt
with elliptic;
k_s/k_n have b

NINE DISC

A test on
radii of the
is enclosed
illustrate hc
The display
reproduced

The norm
ment of thi:
tortion and

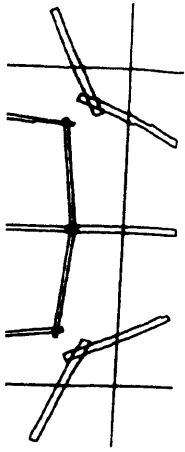*Undistorted*

The bou
ward at a cc
is stopped
tact force.

Damping e

The effe
calculation
tion of the
contact da
tude of ap
global dan
separately
of the forc
brium. A
the walls ;
towards e;

Speed of

The effe
7(a) corre

---

[2] This ran;

in the examples presented here; however, if the physical quantities are known, they may be used in BALL. To interpret the output of BALL, contact forces are displayed graphically. This is done by plotting rectangles through the contacts and with the orientation of the contact forces (see Fig. 5(b)). The lengths of the rectangles are equal to the sum of the radii of the discs in contact and the widths are proportional to the magnitudes of the contact forces. Displays produced in this way resemble the force diagrams obtained from tests on photoelastic discs (see De Josselin de Jong and Verruijt, 1969).

The values of two parameters are chosen with a regard for the properties of physical discs: the interparticle friction angle, ϕ_μ, and the ratio of shear and normal stiffnesses, k_s/k_n. According to analytical results obtained by Mindlin (1949), the ratio k_s/k_n for elastic bodies in contact with elliptical contact areas is in a range from $\frac{2}{3}$ to 1.[2] On the basis of this result, the values of k_s/k_n have been restricted to this range in the tests.

NINE DISC TEST

A test on a regular loosely packed assembly of nine discs is performed as an example. The radii of the discs are 50 units and the density of the disc material is 1000 units. The assembly is enclosed in a square formed by four rigid walls, see Fig. 5(a). The purpose of the test is to illustrate how contact forces develop with time as a function of input parameters and loading. The display of contact forces obtained by moving the walls towards each other uniformly is reproduced in Fig. 5(b).

The normal force at contact C of Fig. 5(a) is selected for a closer examination. The development of this force for various tests is discussed below, firstly for volume decrease without distortion and secondly, for distortion.

Undistorted compression

The boundary conditions for the tests on undistorted compression are that the walls move inward at a constant velocity until 40 calculation cycles have been completed. The wall movement is stopped at this point, but the test is continued, to observe subsequent behaviour of the contact force.

Damping effects

The effect of damping is shown in Fig. 6 where the contact force at C is plotted against the calculation cycles. The plot starts at 40 cycles, the cycle count corresponding to the termination of the wall movement. Curve 1 in Fig. 6 is associated with a case in which neither global nor contact damping operates. The force oscillates about the equilibrium value F_{eq} with an amplitude of approximately $0.15F_{eq}$. Curve 2 in Fig. 6 applies to a case in which both contact and global damping are used. Similar curves are obtained if contact and global damping are used separately. It appears from the figures that the dampling does not affect the equilibrium value of the force. It does, however, reduce the number of calculation cycles needed to reach equilibrium. An interesting feature of the test illustrated in Fig. 5 is that shear forces appear along the walls as a result of relative movement between discs and walls, even though the walls move towards each other uniformly.

Speed of loading

The effect of the speed of loading is illustrated in Fig. 7 for two different stiffnesses. Figure 7(a) corresponds to the cases that the normal, k_n, and shear, k_s, stiffnesses are both $1.35*10^9$.

---

[2] This range applies if the shear force is in the direction of the minimum diameter of the contact area.
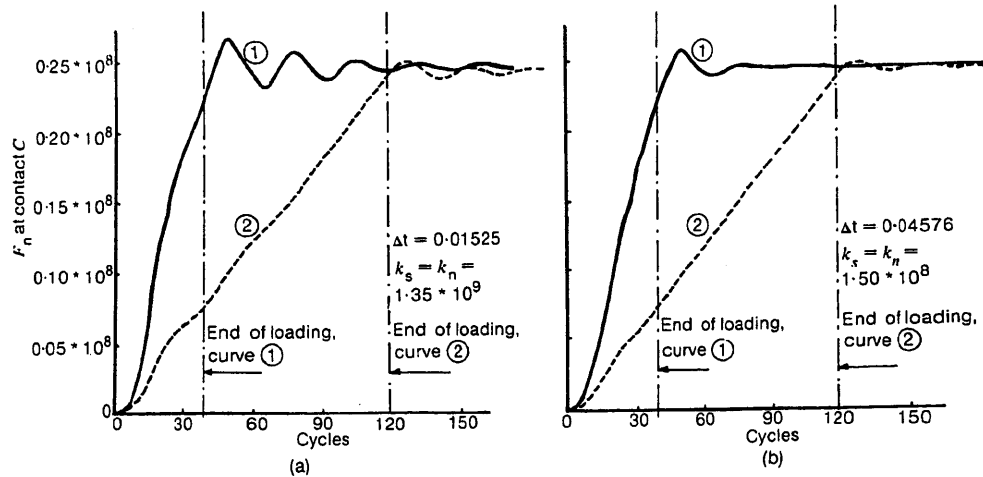
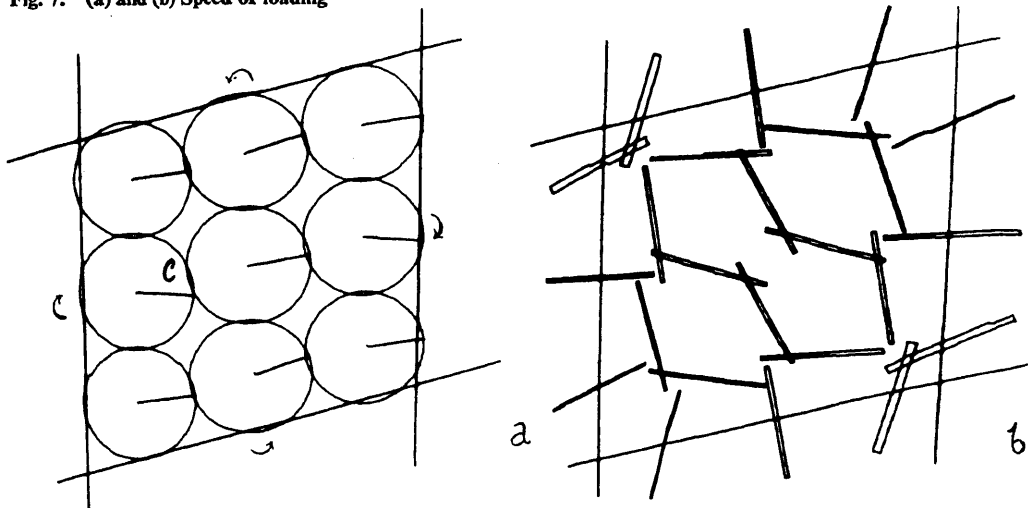Fig. 7. (a) and (b) Speed of loading

Fig. 8. Constant volume strain

Curves 1 and 2 apply to wall velocities of 0·12 and 0·04, respectively. The deformations for the two tests have been chosen such that about the same equilibrium force results; the number of calculation cycles at the end of loading for the wall velocity of 0·04 is three times that for the wall velocity of 0·12. It is seen that the amplitude of the oscillations occurring at the end of loading is much larger for curve 1 (high speed) than for curve 2 (low speed), whereas the frequencies are about the same. Thus, the amplitude of the oscillations occurring at the end of loading increases with the speed of loading. The same effect is observed in the graphs of Fig. 7(b), corresponding to $k_n = k_s = 1·50*10^8$. Curve 1 applies to a loading speed of 0·36 and curve 2 to a loading speed of 0·12. The loading has been continued up to a compression that yields the same equilibrium force as for the low-stiffness case of Fig. 7(a).

The oscillations are smaller for a low speed than for a high speed of loading because other accelerations induced in the particles decrease with decreasing speed of loading. If the inertial

Fig. 9. The effect of k

forces are kept low at all times. For a the speed of loadir

Distortion

To illustrate th point C, the comp specifying a cons1 global and contac assembly remains the assembly are

Shear to normal s

The effects of t at contact C are il The normal and all curves is 1·35 $= \frac{1}{3}$ and $k_s/k_n =$ that the influenc be that slip sets slip sets in, the however, where test and the cui case of the hig pression is less t shear stresses di

Δt = 0·04576
$k_s = k_n =$
1·50 * 10⁸

End of loading,
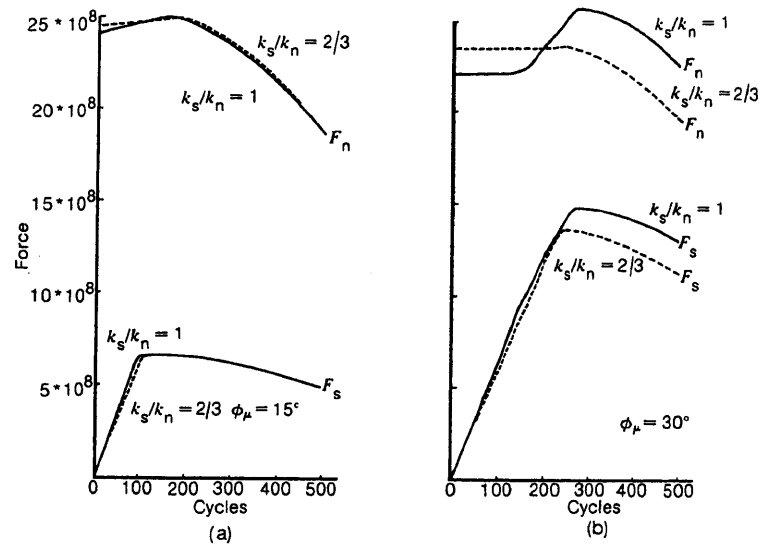curve ②

ig,

0   120   150
les

)

Fig. 9.   The effect of k_s/k_n and ϕ_μ on the contact force at c

forces are kept low compared to the contact forces, the system will remain close to equilibrium at all times. For a more detailed discussion of the effects of the various forms of damping and of the speed of loading on the behaviour of the assembly see Cundall (1978).

Distortion

To illustrate the effects of the ratio k_s/k_n and the friction angle ϕ_μ on the contact force at point C, the compressed assembly is subjected to distortion, at constant volume. This is done by specifying a constant angular velocity about the wall centres, as indicated in Fig. 8(a). Both global and contact damping are applied and the speed of loading is kept low to ensure that the assembly remains close to a state of equilibrium at all times. The contact forces generated in the assembly are reproduced in Fig. 8(b).

Shear to normal stiffness ratio and friction angle

The effects of the ratio k_s/k_n and the friction angle ϕ_μ on the normal (F_n) and shear (F_s) forces at contact C are illustrated in Figs 9(a) and (b), corresponding to 15° and 30° for ϕ_μ, respectively. The normal and shear forces are plotted against the calculation cycles and the value for k_n for all curves is $1·35*10^9$, i.e. the ratio k_s/k_n is changed by varying k_s only. The curves for $k_s/k_n = \frac{2}{3}$ and $k_s/k_n = 1$ nearly coincide for the case that $\phi_\mu = 15°$ (see Fig. 9(a)). The explanation that the influence of the value of k_s/k_n upon F_n and F_s for small friction angles is minor may be that slip sets in early and controls the shear force for a major portion of the test; as soon as slip sets in, the shear force is determined solely by the normal force. For the case of Fig. 9(b) however, where $\phi_\mu = 30°$, the shear stiffness controls the behaviour over a longer portion of the test and the curves for $k_s/k_n = \frac{2}{3}$ and for $k_s/k_n = 1$ are seen to deviate significantly. For the case of the high shear stiffness, $k_s/k_n = 1$, the value for F_n resulting from undistorted compression is less than for the case that $k_s/k_n = \frac{2}{3}$ (see Fig. 9(b)). Even for undistorted compression, shear stresses develop at the boundaries as a result of movement of discs along the walls. These
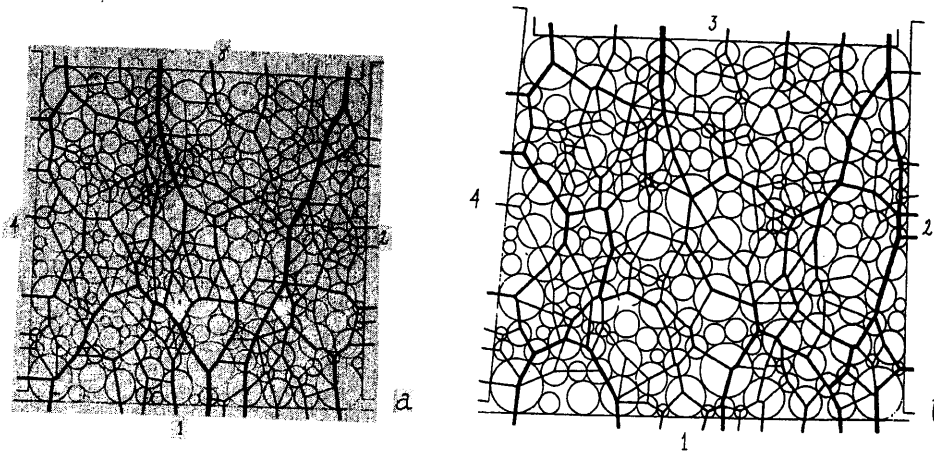
leformations for the
ults; the number of
e times that for the
irring at the end of
d), whereas the fre-
irring at the end of
graphs of Fig. 7(b),
of 0·36 and curve 2
ssion that yields the

iding because other
ling. If the inertial

Fig. 10. Force vector plots obtained by De Josselin de Jong and Verruijt (1969); (a) Stage A, ratio $F_H/F_v = 0.39$: (b) Stage B, ratio $F_H/F_v = 0.33$

Fig. 11. Numeric
B, ratio $F_H/F_v = 0$

Fig. 12. Numeric
B, ratio $F_H/F_v = 0$

shear stresses carry part of the load and are higher, the higher the ratio of k_s to k_n. This explains the difference in initial values for F_n. However, as shearing proceeds, the normal force for the case that $k_s/k_n = 1$ increases beyond the one for $k_s/k_n = \frac{2}{3}$ to reach a maximum of about $25.6*10^8$ after which slip sets in and the force falls back.

It follows from the above results that the parameters k_s/k_n and ϕ_μ have a considerable influence upon the behaviour of the assembly. Therefore, care has been taken in estimating friction angles for the comparison against results of tests on photoelastic discs. In addition, the ratio k_s/k_n has been varied between $\frac{2}{3}$ and 1 and tests with different friction angles have been performed.

In addition to the experiments discussed above as illustrative examples, experiments were performed to investigate the effect of changes in the values of k_s and k_n, keeping the ratio k_s/k_n constant, upon the behaviour of the assemblies. It appears that assemblies of very stiff particles behave quite differently from assemblies of soft particles. This may be understood physically: a material of particles that deform easily (i.e. particles with a small value for k_n) is expected to respond in a different way to loading than a material of stiff particles (e.g. sand).

It should be noted that the force–displacement law currently used in BALL is a rather simple one. Investigation into the effect of changes made in these laws upon the behaviour of the assembly will indicate whether it will be necessary to refine the model. However, the results of the verification tests discussed below, qualitative as they are, indicate that the model is quite realistic in its present form.

VERIFICATION TEST

An attempt is made to duplicate numerically the test on photoelastic discs described by De Josselin de Jong and Verruijt (1969). The assembly of discs was placed between two vertical Plexiglas plates and was loaded by means of two horizontal and two vertical rigid beams which formed the side boundaries. The horizontal beams were subjected to vertical forces and the vertical beams to horizontal forces. All beams were free to rotate. De Josselin de Jong and Verruijt present figures with disc locations and contact forces for two stages of the test, referred to in this Paper as stages A and B. These figures are reproduced as Figs 10(a) and (b). At stage A the ratio F_H/F_v of the forces applied in the horizontal (F_H) and vertical (F_v) directions was
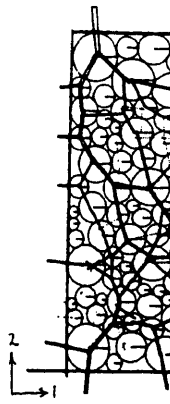
0.39. The tran
4.348 % while d

The purpose
presented by D
interpreting the

The discs' cer
centre points of
to the grid in th
dure results in
invisibility of th

The density t
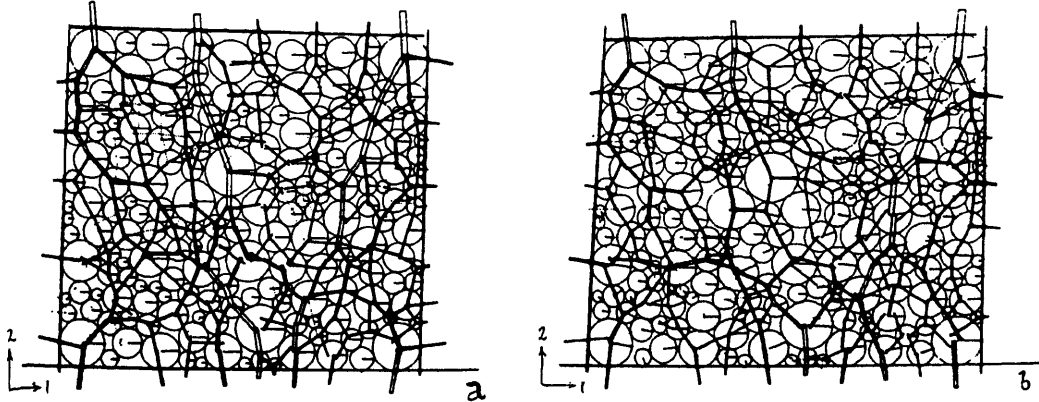there are 6 disc
of 10 units.

The disc-to-
obliquity of th

Fig. 11. Numerical reproduction of Fig. 10, with data from Table 1; (a) Stage A, ratio $F_H/F_v = 0.43$; (b) Stage B, ratio $F_H/F_v = 0.40$
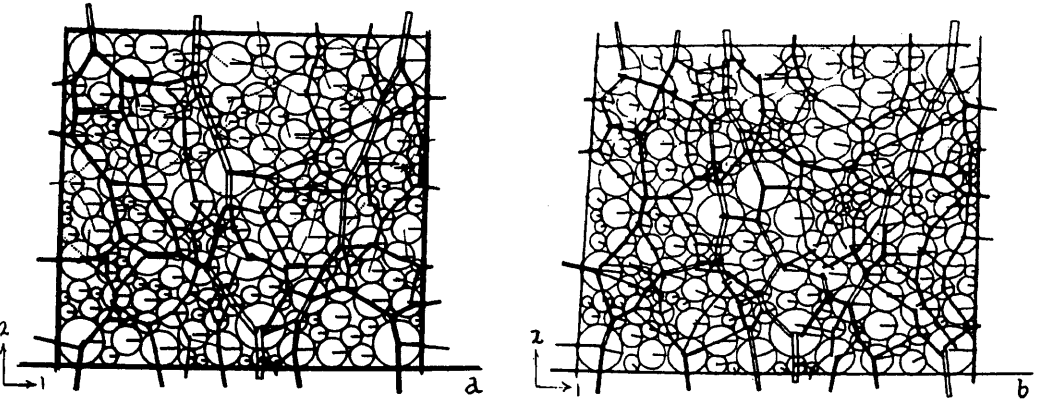

Fig. 12. Numerical reproduction of Fig. 10, with data from Table 2; (a) Stage A, ratio $F_H/F_v = 0.41$: (b) Stage B, ratio $F_H/F_v = 0.40$

0.39. The transition from stage A to stage B was made by increasing the vertical force by 4.348 % while decreasing the horizontal force by the same amount, yielding a ratio F_H/F_v of 0.33.

The purpose of the verification is to compare force vector plots produced by BALL with those presented by De Josselin de Jong and Verruijt. The verification is primarily qualitative, and, in interpreting the results, heavy emphasis is placed upon visual comparison.

The discs' centre locations and radii were obtained from Fig. 10(a) by use of a digitizer. The centre points of the discs, marked by cross-hairs in the original test, were located with reference to the grid in the background of the photograph. It may be noted that use of the above procedure results in an approximate geometry of the assembly as errors are caused by occasional invisibility of the cross-hairs and by distortions in the figure.

The density used for the discs is taken as 2000 units and the sizes of the discs are as follows: there are 6 discs of a radius of 40, 7 of 35, 16 of 30, 33 of 25, 33 of 20, 36 of 18, 28 of 15 and 38 of 10 units.

The disc-to-disc and disc-to-wall friction angles are determined by measuring the largest obliquity of the contact forces. This is done under the assumption that the largest obliquity

Table 1. Data for Fig. 11. The wall numbers are as labelled in Fig. 10

Stage	A				B			
Wall No.	1	2	3	4	1	2	3	4
F_1 (→)	$+0.2836*10^8$	$-0.3040*10^9$	$+0.3790*10^8$	$+0.2386*10^9$	$-0.6240*10^8$	$-0.8445*10^9$	$+0.2848*10^8$	$+0.8770*10^9$
F_2 (↑)	$+0.6337*10^9$	$-0.1843*10^7$	$-0.6260*10^9$	$-0.8954*10^7$	$+0.2111*10^{10}$	$+0.5217*10^8$	$-0.2169*10^{10}$	$+0.1092*10^6$
$(e/\frac{1}{2}L)*100\%$[1]	7·95%	1·52%	5·25%	0·84%	14·5%	4·88%	16·5%	4·19%
$(\Delta F/F)*100\%$[2]	$(0·1872*10^7/0·2009*10^9)*100\% = 0·9\%$				$(0·5872*10^6/0·7365*10^9)*100\% = 0·1\%$			

Key: k_n = 1·5*10^9, k_s = 1·0*10^9, $(\tan \phi_\mu)_{dd}$ = 0·45, $(\tan \phi_\mu)_{dw}$ = 0·17.
[1] $e/(\frac{1}{2}L)$ represents the eccentricity of the force acting normal to the wall divided by half the wall length.
[2] $\Delta F/F$ represents the ratio of the largest force-sum on any disc to the largest contact force.
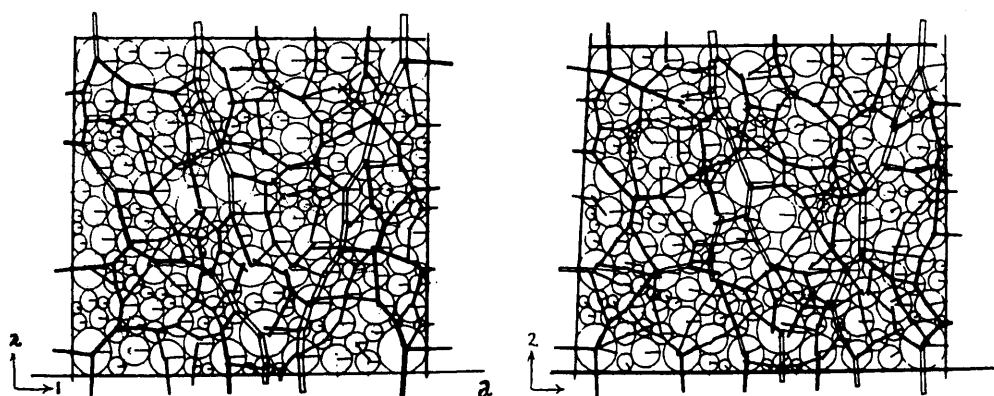
Fig. 13. Numerical reproduction of Fig. 10, with data from Table 3; (a) Stage A, ratio $F_H/F_v = 0.46$; (b) Stage B, ratio $F_H/F_v = 0.47$

observed equals the maximum possible obliquity. The resulting value for all disc-to-disc contacts is $(\tan \phi_\mu)_{dd} = 0.45$ and the value for all disc-to-wall contacts is $(\tan \phi_\mu)_{dw} = 0.17$.

A difficulty in reproducing the photoelastic disc test is that the geometry of the assembly and the wall locations as they existed before loading are unknown. Therefore, the geometry of Fig. 10(a) is used as the initial configuration. The four walls are translated inward in such a way that the ratio of vertical and horizontal resultant wall forces approximates to the original value. The transition from stage A to stage B is made by moving the four walls to the positions indicated in Fig. 10(b). It may be noted that the above procedure differs from the one used for the photoelastic analysis in two respects. Firstly, the initial conditions deviate somewhat from those of the original test and secondly, the numerical test is strain-controlled whereas the original is stress-controlled.

The vector plot and disc locations obtained numerically for stages A and B are reproduced in Figs 11(a) and (b) for the case that $(\tan \phi_\mu)_{dd} = 0.45$, $(\tan \phi_\mu)_{dw} = 0.17$ and $k_s/k_n = \frac{2}{3}$. Keeping in mind the approximations made, the resemblance is good. The boundary forces obtained numerically are listed in Table 1. The ratios of horizontal over vertical forces deviate somewhat from the original ones as a result of the discrepancy in boundary and initial conditions. The boundary forces are given in terms of components F_1 and F_2, taken positive in the directions of the 1 and 2 axes indicated in the figure.

To investigate the effect of the ratio k_s/k_n upon the force vector plots, the test is repeated for the case that $k_s = k_n$. The force vector plots and disc locations are reproduced in Figs 12(a) and (b).

Finally, the results are presented in Figs 13(a) and (b) of a test with friction angles that are slightly less than for the above test: $(\tan \phi_\mu)_{dd} = 0.40$, $(\tan \phi_\mu)_{dw} = 0.08$. The shear and normal stiffnesses are both taken as $1.5*10^9$. The boundary forces and moments are listed in Table 3.

CONCLUSION

The above verification is primarily qualitative and therefore subjective. Nonetheless, the correspondence between numerically and photoelastically obtained force vector plots is sufficiently good to conclude that the distinct element method is a valid tool for fundamental research into the behaviour of granular assemblies.

Table 2. Data for Fig. 12

Stage	A				B			
Wall No.	1	2	3	4	1	2	3	4
F_1 (→) F_2 (↑) $(e/\frac{1}{2}L)*100\%$	$-0.2093*10^7$ $+0.7372*10^8$ 5.90%	$-0.2981*10^8$ $-0.1542*10^6$ 6.60%	$-0.1469*10^7$ $-0.6987*10^8$ 1.44%	$+0.2962*10^8$ $-0.1493*10^7$ 0.06%	$-0.5063*10^8$ $+0.1437*10^{10}$ 4.63%	$-0.5536*10^9$ $+0.2766*10^8$ 2.72%	$-0.2592*10^7$ $-0.1446*10^{10}$ 9.03%	$+0.6039*10^9$ $+0.1809*10^8$ 1.03%
$(\Delta F/F)*100\%$	$(0.7462*10^6/0.2835*10^8)*100\% = 2.6\%$				$(0.4494*10^6/0.4136*10^9)*100\% = 0.1\%$			

Key: $k_n = k_s = 1.5*10^9$, $(\tan \phi_\mu)_{dd} = 0.45$, $(\tan \phi_\mu)_{dw} = 0.17$.

Table 3. Data for Fig. 13

Stage	A				B			
Wall No.	1	2	3	4	1	2	3	4
F_1 (→) F_2 (↑) $(e/\frac{1}{2}L)*100\%$	$+0.1774*10^7$ $+0.2963*10^9$ 12.79%	$-0.1468*10^9$ $-0.4272*10^6$ 5.22%	$+0.8015*10^7$ $+0.2972*10^9$ 10.92%	$+0.1254*10^9$ $-0.4042*10^7$ 0.66%	$-0.3588*10^8$ $+0.1725*10^{10}$ 13.26%	$-0.8002*10^9$ $+0.1003*10^8$ 5.29%	$+0.8067*10^7$ $-0.1694*10^{10}$ 13.23%	$+0.8182*10^9$ $-0.4016*10^8$ 3.54%
$(\Delta F/F)*100\%$	$(0.1617*10^7/0.9375*10^8)*100\% = 1.7\%$				$(0.2902*10^7/0.5037*10^9)*100\% = 0.6\%$			

Key: $k_n = k_s = 1.5*10^9$, $(\tan \phi_\mu)_{dd} = 0.40$, $(\tan \phi_\mu)_{dw} = 0.08$.

REFERENCES

Cundall, P. A. (1971). A computer model for simulating progressive, large-scale movements in blocky rock systems. *Proc. Symp. Int. Soc. Rock Mech., Nancy* 2, No. 8.

Cundall, P. A. (1974). *A computer model for rock–mass behavior using interactive graphics for the input and output of geometrical data.* Report MRD–2–74 prepared at the University of Minnesota under Contract number DACW 45–74–C–006, for the Missouri River Division, US Army Corps of Engineers, available from National Technical Information Service—report number AD/A–001 602.

Cundall, P. A. (1978). *BALL—A program to model granular media using the distinct element method.* Technical Note, Advanced Technology Group, Dames & Moore, London.

Dantu, P. (1957). Contribution á l'étude mécanique et géomtrique des milieux pulvérulents. *Proc. 4th Int. Conf. Soil Mech. Fdn Engng, London* 1, pp. 144.

De Josselin de Jong, G. & Verruijt, A. (1969). Etude photo-élastique d'un empilement de disques. *Cah. Grpe fr. Etud. Rhéol.* 2, 73–86.

Deresiewicz, H. (1958). Mechanics of granular material. *Advd. appl. Mech.* 5, 233–306.

Drescher, A. & De Josselin de Jong, G. (1972). Photoelastic verification of a mechanical model for the flow of a granular material. *J. Mech. Phys. Solids* 20, 337–351.

Mindlin, R. D. (1949). Compliance of elastic bodies in contact. *J. appl. Mech.* 71, No. 3, 259–268.

Mindlin, R. D. & Deresiewicz, H. (1953). Elastic spheres in contact under varying oblique forces. *J. Appl. Mech.* 20, 327–344.

Nayak, P. R. (1972). Surface roughness effects in rolling contact. *Trans. Am. Soc. mech. Engrs* Series E, *J. Appl. Mech.* 39, No. 2, 456–460.

Rodriguez-Ortiz, J. M. (1974). Estudio del comportamiento de medios granulares heterogéneos mediante modelos discontinuos analógicos y matemáticos. PhD thesis, Universidad Politécnica de Madrid.

Serrano, A. A. & Rodriguez-Ortiz, J. M. (1973). A contribution to the mechanics of heterogeneous granular media. *Proc. Symp. Plasticity and Soil Mech., Cambridge.*

Strack, O. D. L. & Cundall, P. A. (1978). *The distinct element method as a tool for research in granular media.* Report to National Science Foundation from Department of Civil and Mineral Engineering, University of Minnesota, USA.

Wakabayashi, T. (1957). Photoelastic method for determination of stress in powdered mass. *Proc. 7th Jap. Nat. Congr. Appl. Mech.* 153–192.

	$(e/\frac{1}{2}L)*100\%$	$(\Delta F/F)*100\%$
$+0.8182*10^9$ $-0.4016*10^8$ 3·54%		
$+0.8067*10^7$ $-0.1694*10^{10}$ 13·23%		$(0.2902*10^7/0.5037*10^9)*100\% = 0.6\%$
$-0.8002*10^9$ $+0.1003*10^8$ 5·29%		
$-0.3588*10^8$ $+0.1725*10^{10}$ 13·26%		
$+0.1254*10^9$ $-0.4042*10^7$ 0·66%		$(0.1617*10^7/0.9375*10^8)*100\% = 1.7\%$
$-0.2972*10^9$ 10·92%		
$-0.4272*10^6$ 5·22%		
$+0.2963*10^9$ 12·79%		

Key: $k_n = k_s = 1.5*10^9$, $(\tan \phi_\mu)_{dd} = 0.40$, $(\tan \phi_\mu)_{dw} = 0.08$